

Evaluation of ^{11}C -LSN3172176 as a novel PET tracer for imaging M_1 muscarinic acetylcholine receptors in non-human primates

Nabeel B. Nabulsi¹, Daniel Holden¹, Ming-Qiang Zheng¹, Frederic Bois¹, Shu-Fei Lin¹, Soheila Najafzadeh¹, Hong Gao¹, Jim Ropchan¹, Teresa Lara-Jaime¹, David Labaree¹, Anupama Shirali¹, Lawrence Sliker², Cynthia Jesudason², Vanessa Barth², Antonio Navarro², Nancy Kant², Richard E. Carson¹, Yiyun Huang¹

¹Yale PET Center, Department of Radiology and Biomedical Imaging, Yale University, New Haven, CT, USA

²Eli Lilly and Co., Indianapolis, Indiana, USA

Name and Address for Correspondence:

Nabeel B. Nabulsi, Ph.D.

Yale PET Center

P.O. Box 208048

Yale School of Medicine

New Haven, CT 06520

USA

Telephone: 203-785-2474

Fax: 203-785-2978

Email: nabeel.nabulsi@yale.edu

Total Word count: 4997 (limit 5000 total including title page, abstract, text, disclosure, acknowledgments, references, figure legends, and tables)

Words in abstract: 321 (limit 350)

Short running foot line: M₁ mAChR PET Imaging in Nonhuman Primate

Keywords: Muscarinic, M₁, ¹¹C-LSN3172176, Scopolamine, Nonhuman primate.

ABSTRACT

The M₁ muscarinic acetylcholine receptor (mAChR) plays an important role in learning and memory, and therefore is a target for development of drugs for treatment of cognitive impairments in Alzheimer's disease and schizophrenia. The availability of M₁-selective radiotracers for positron emission tomography (PET) will help in developing therapeutic agents by providing an imaging tool for assessment of drug dose-receptor occupancy relationship. Here we report the synthesis and evaluation of ¹¹C-LSN3172176 (ethyl 4-(6-(methyl-¹¹C)-2-oxoindolin-1-yl)-[1,4'-bipiperidine]-1'-carboxylate) in non-human primates.

Methods: ¹¹C-LSN3172176 was radiolabeled via the Suzuki-Miyaura cross-coupling method. PET scans in rhesus macaques were acquired on the Focus-220 for 2 h with arterial blood sampling and metabolite analysis to measure the input function. Blocking scans with scopolamine (50 µg/kg) and the M₁-selective agent AZD6088 (0.67 and 2 mg/kg) were performed to assess tracer binding specificity and selectivity. Regional brain time-activity curves (TACs) were analyzed with the one-tissue (1T) compartment model and the multilinear analysis method (MA1) to calculate regional distribution volume (V_T). Non-displaceable binding potential (BP_{ND}) values were calculated using the cerebellum as reference region.

Results: ¹¹C-LSN3172176 was synthesized with >99% radiochemical purity and high molar activity. In rhesus monkeys ¹¹C-LSN3172176 metabolized rapidly ($29 \pm 6\%$ parent remaining at 15 min), and displayed fast kinetics and extremely high uptake in the brain. Imaging data were modeled well with the 1T and MA1 methods. MA1-derived V_T values were high (range of 10-81 mL/cm³) in all known M₁ mAChR-rich brain regions. Pre-treatment with scopolamine and AZD6088 significantly reduced the brain uptake of ¹¹C-LSN3172176, thus demonstrating its binding specificity and selectivity *in vivo*. The cerebellum appeared to be a suitable reference region for derivation of BP_{ND} , which ranged from 2.42 in the globus pallidus to 8.48 in the nucleus accumbens.

Conclusion: ¹¹C-LSN3172176 exhibits excellent *in vivo* binding and imaging characteristics in non-human primates and appears to be the first appropriate radiotracer for PET imaging of human M₁ AChR.

Keywords: M1 AChR, PET, radioligand, ¹¹C-LSN3172176, non-human primates, scopolamine.

INTRODUCTION

The muscarinic acetylcholine receptors (mAChRs) are G protein-coupled receptors (GPCRs) widely expressed in the central nervous system (CNS), where they mediate acetylcholine (ACh) neurotransmission (1), and thus are targets for drug discovery (2). Five main subtypes of mAChRs (M₁-M₅) have been identified. The M₁ receptor is abundantly expressed throughout the striatum, cortex, hippocampus and amygdala (3-6). These regions are important for learning and memory, and to develop amyloid plaques in Alzheimer's disease patients (7). Many studies showed that M₁-knockout mice display cognitive deficits (3,8-10), and activation of the M₁ mAChR had precognitive effects (8,11-13), improving memory and modulating hippocampal synaptic plasticity (13-20).

Given the important roles of M₁ mAChR in regulating memory, cognition, and behavior, selective M₁ activation has emerged as a potential treatment strategy for cognitive impairments in Alzheimer disease and schizophrenia (21-24). Therapeutic application of non-selective mAChR agonists, e.g., melameline, sabcomeline, and xanomeline, has been limited by cholinergic adverse events such as diarrhea, nausea, gastrointestinal anomalies, salivation, and sweating thought to be mediated by mAChR subtypes other than M₁ (25). Therefore there remains a need for developing M₁-selective drugs for potential treatment of cognitive disorders.

Positron emission tomography (PET) ligands that selectively bind to a target would greatly facilitate discovery of drugs with minimal to no side effects for superior therapeutic applications. Several PET ligands with affinity to M₁ have been reported, e.g., ¹¹C-scopolamine (26), ¹¹C-NMPB (27), *N*-methyl ¹¹C-benztropine (28) and ¹¹C-QNB (29) (Fig. 1). These ligands have good brain uptake and were employed to map mAChR in primate brains. However, they lack M₁ selectivity, and display slow or irreversible binding kinetics. ¹¹C-Xanomeline, and the M₁ allosteric agonist ¹¹C-GSK-1034702 are among the available nonselective agonist PET ligands exhibiting limited specific binding despite clear brain penetration (30,31). ¹¹C-AF150(S) was recently reported as an agonist PET ligand for M₁ receptors and evaluated in rats (32,33). However, the authors concluded that its use in brain imaging would be

challenging due to its low lipophilicity (log D of 0.050), rapid metabolism, and moderate affinity (K_d of 200 nM for M_1 in rat cerebral cortex) (32). More recently, (*S*)-1-(methyl- ^{11}C)piperidin-3-yl (*R*)-2-cyclopentyl-2-hydroxy-2-phenylacetate was reported as a high affinity ($K_i = 3.5$ nM) radioligand based on the chemical scaffold of the antagonist MPB, but it appears to possess limited *in vivo* binding specificity, as its uptake was only partially blocked by the M_1 selective antagonist pirenzepine (34).

We recently reported the discovery of two novel M_1 mAChR selective agonist ligands, LSN3172176 and LSN3262527 (Fig. 2), which are amenable to ^{11}C -radiolabeling, (35,36). Here we report the radiosynthesis of ^{11}C -LSN3172176 (ethyl 4-(6-(methyl- ^{11}C)-2-oxoindolin-1-yl)-[1,4'-bipiperidine]-1'-carboxylate) and its *in vivo* characterization in non-human primates.

MATERIALS AND METHODS

Both the reference standard LSN3172176 and the boronic acid precursor LSN3234794 were prepared by Eli Lilly & Company (Lilly Research Centre, Windlesham, UK) according to published procedures (37). Fig. 3 outlines brief synthetic schemes for LSN3172176 and LSN3234794, including radiosynthesis of ^{11}C -LSN3172176. See supplemental material for details.

In Vitro and In Vivo Properties

All *in vitro* pharmacological characterization and *in vivo* validation of LSN3172176 as an M_1 -selective mAChR PET tracer was described recently (38). EC_{50} values are 7.0 nM, 3.7 nM and 2.4 nM in mouse, rat, and human, respectively. Binding affinity (K_i , nM) for mAChRs is in the following rank order: M_1 (8.9) \gg M_4 (41.4) $>$ M_5 (55.6), M_2 (63.8) $>$ M_3 (3,031).

PET Imaging Experiments in Rhesus Monkeys

General PET Study Design. Imaging experiments were carried out in rhesus monkeys (*Macaca mulatta*) according to a protocol approved by the Yale University Institutional Animal Care and Use Committee and procedures. Two sets of scans were performed: (1) baseline with ^{11}C -LSN3172176 followed by a blocking scan after administration of 50 $\mu\text{g}/\text{kg}$ scopolamine over 10 min at about 40 min

before the start of the second scan ($n=2$); (2) two blocking scans with ^{11}C -LSN3172176 after pre-treatment with the known M_1 selective partial agonist AZD6088 at the doses of 0.67 and 2 mg/kg, both given over 15 min at about 2 h before the injection of ^{11}C -LSN3172176.

PET scan and image analysis procedures. Subjects were sedated ~2 h before the first PET scan and kept anesthetized for the duration of the experiments as previously described (39).

Brain images were acquired using the FOCUS 220 PET scanner (Siemens Preclinical Solutions, Knoxville, TN) with a reconstructed image resolution of ~1.5 mm. Following a transmission scan, ^{11}C -LSN3172176 was injected intravenously over 3-min using an infusion pump as reported previously (39). List-mode data were acquired for 120 min and binned into sinograms with the following frame timing: 6×30 sec; 3×1 min; 2×2 min; and 22×5 min.

Scan data were reconstructed with a FORE/filtered back projection algorithm as described previously (39). Regions of interest (ROIs, $n=16$) were previously delineated on a single representative anatomical rhesus monkey magnetic resonance image (MRI) registered to a template image. Regions used in this study were amygdala, brainstem, caudate, cerebellum, cingulate cortex, frontal cortex, globus pallidus, hippocampus, insula, nucleus accumbens (nacc), occipital cortex, pons, putamen, substantia nigra, temporal cortex and the thalamus. Registration parameters (from PET-to-MR and from MR-to-atlas) were obtained to apply the ROIs to individual PET scans (40), and regional time-activity curves (TACs) were generated and expressed in standardized uptake value (SUV) by normalizing by the injected dose and animal body weight.

Metabolite Analysis, Arterial Input Function and Log D Determination. Arterial blood samples were collected to determine the unmetabolized parent fraction using the automatic column-switching HPLC system (41), and to calculate the plasma input function. The plasma free fraction (f_p) was measured in triplicate using the ultrafiltration method, and the log D was determined by modification of the previously published procedure (42). Additional details are provided in the supplemental material.

Data Analysis. Regional brain TACs were analyzed with the one-tissue (1T) compartment model. Fit quality was compared to the two-tissue (2T) compartment model and the multilinear analysis-1 (MA1) method (43) to calculate the distribution volume (V_T). In MA1, data were fitted starting at time $t^* = 30$ min. Regional BP_{ND} values were calculated using MA1 V_T values with cerebellum as the reference region (44). The simplified reference tissue model (SRTM) (45) was also used to calculate regional BP_{ND} values with cerebellum as the reference region.

For the blocking experiments, target occupancy was estimated using the Lassen plot approach, which can determine the nondisplaceable volume of distribution (V_{ND}) and receptor occupancy using V_T values at baseline and after pretreatment (46).

RESULTS

Radiochemistry

^{11}C -LSN3172176 was synthesized via Pd^0 -mediated cross-coupling of ^{11}C -iodomethane (47) with 1 – 1.2 mg of the boronic acid precursor (48,49) in $49.3 \pm 16.6\%$ radiochemical yield (decay-corrected) at the end of beam (EOB) based on trapped ^{11}C -iodomethane radioactivity ($n = 12$). The radiochemical purity was $> 99\%$, and the average molar activity (A_m) was 422 ± 259 MBq/nmol at the end of synthesis (EOS). Total synthesis time was 47 ± 5 min from EOB. The radiochemical purity remained $>98\%$ at 60 min after EOS. See supplemental material for details.

PET Scans in Rhesus Monkeys

The mean injected dose of ^{11}C -LSN3172176 was 187 ± 3 MBq, with A_m of 225 ± 100 MBq/nmol at the time of injection and injected mass was 0.041 ± 0.018 $\mu\text{g}/\text{kg}$.

Plasma Analysis. Parent fraction and radioactivity in plasma over time are presented in Fig. 4. ^{11}C -LSN3172176 metabolized rapidly. The parent fraction accounted for $29 \pm 6\%$ of the radioactivity at 15 min post-injection, which decreased to $10 \pm 3\%$ at 90 min ($n = 8$). All radiometabolites were more polar

than the parent compound (Supplemental Fig. 1: retention times ~3 and 7 min, compared to ~ 11 min for the parent). The plasma free fraction (f_p) was high, at $41 \pm 3 \%$ ($n = 12$). The measured $\log D$ of ^{11}C -LSN3172176 was 2.96 ± 0.02 , in the optimal range (1-3.5) for brain PET radiotracers (50).

Image Analysis and Kinetic Modeling. Representative brain PET images summed from 30 to 45 min after tracer injection are shown in Fig. 5. At baseline, high uptake was seen throughout the brain (Fig. 5A), with SUV highest in the striatum followed by cortical regions, and lowest in the cerebellum. Pretreatment with the nonselective mAChR antagonist scopolamine (50 $\mu\text{g}/\text{kg}$) markedly decreased radioactivity uptake (Fig. 5B), confirming *in vivo* binding specificity of ^{11}C -LSN3172176. Likewise, blockade by the M_1 -selective partial agonist AZD6088 (2 mg/kg) confirmed ^{11}C -LSN3172176 *in vivo* selectivity for M_1 mAChR (Fig. 5C).

Regional brain TACs are presented in Fig. 6. ^{11}C -LSN3172176 displayed very high uptake and reversible kinetics, with peak SUV of 4 to 9.5 and peak uptake time ranging from 10-50 min post administration (Fig. 6A). Pretreatment with 50 $\mu\text{g}/\text{kg}$ scopolamine reduced uptake across all regions to levels similar to that in the cerebellum, with regional radioactivity peaking earlier and clearing faster (Fig. 6B). Similarly, pretreatment with 2 mg/kg of AZD6088 reduced uptake in all brain regions to more homogeneous levels demonstrating target selectivity (Fig. 6C).

It is known that the cerebellum is almost devoid of mAChRs (51,52). Indeed, uptake in the cerebellum did not change significantly between baseline and scopolamine blocking scans (Fig. 6B), supporting the use of cerebellum as reference region.

The 1T model produced suitable but less than ideal fits of regional TACs. MA1 ($t^* = 30$) produced good fits and stable estimates of V_T values well correlated with those from 1T (Supplemental Fig. 2). Overall, 2T did not provide reliable V_T values, with the majority of the estimates having SEs of $>25\%$ (data not shown). Thus, MA1 was chosen for analysis.

Table 1 presents regional V_T values derived from MA1. V_T values are higher in the striatal (putamen, nucleus accumbens, and caudate) and cortical areas, moderate in the hippocampus, amygdala, and globus

pallidus, and lower in other regions. Dramatic reduction in regional V_T was seen with administration of scopolamine (50 $\mu\text{g}/\text{kg}$). Likewise, pre-blocking with two doses of AZD6088 resulted in a clear and dose-dependent reduction in regional V_T . Regions with low V_T estimates (pons, brainstem and cerebellum) displayed negligible changes. The average receptor occupancy calculated from the occupancy plot was 98.6% by 50 $\mu\text{g}/\text{kg}$ scopolamine (Fig. 7). Occupancies of 68% and 89% were found with 0.67 and 2 mg/kg of AZD6088, respectively. The average V_{ND} in the blocking scans with scopolamine and with the two doses of AZD6088 was calculated to be $6.3 \pm 0.8 \text{ mL}/\text{cm}^3$.

Regional BP_{ND} values were calculated from the MA1 V_T values using cerebellum as the reference region (Table 1). Note that the average V_{ND} value of $6.3 \pm 0.8 \text{ mL}/\text{cm}^3$ estimated from the blocking scans is in good agreement with the mean baseline V_T value of $8.1 \pm 1.3 \text{ mL}/\text{cm}^3$ for the cerebellum, indicating the cerebellum may be a suitable reference region. *In vitro* studies showed no significant ^3H -LSN3172176 binding to the cerebellum in monkey tissue and across other species (38). The minimal reduction in cerebellum V_T caused by blockade may be due to partial volume effects from the high uptake in gray matter regions.

Regional BP_{ND} values derived from the SRTM using cerebellum as the reference region are also listed in Table 1. SRTM produced good fits of regional TACs and reliable BP_{ND} estimates. The highest V_T and BP_{ND} observed in the nucleus accumbens are consistent with autoradiographic study of M_1 distribution in the human brain (53). In addition to the role of nucleus accumbens in the reward circuit (54), it is reported to be important in spatial learning and memory as well (55). BP_{ND} values derived from the SRTM method were consistently lower by about 25% across all brain regions (Supplemental Fig. 3A). A scatter plot of SRTM and MA1 BP_{ND} (Supplemental Fig. 3B) for the same selected brain regions showed excellent correlation ($r = 0.998$), with slope of 0.746 and intercept close to zero (0.155). Lower SRTM derived BP_{ND} values are not uncommon for many tracers, due to violation of SRTM assumptions (56).

The MA1 estimated BP_{ND} for the cortical tissue is noteworthy. The measured *in vitro* B_{max} and K_d for ^3H -LSN3172176 binding in rhesus cortex are $843 \pm 69 \text{ fmol}/\text{mg}$ protein ($843 \pm 69 \text{ nM}$) and $8 \pm 3 \text{ nM}$ (n

=3), respectively (38), yielding *in vitro* BP ($=B_{\max}/K_D$) value of 105.4. The average V_{ND} calculated from all four blocking scans (two with scopolamine and two with AZD6088) in this study was 6.3 ± 0.8 mL/cm³, and f_p was 0.41 ± 0.03 . As $BP_{ND} = f_{ND} * B_{\max}/K_D$ and $f_{ND} = f_p/V_{ND} = 0.065$, the *in vitro* BP_{ND} for rhesus cortex would be 6.86, which is in good agreement with the *in vivo* BP_{ND} values for the frontal (5.33), occipital (4.02), and temporal (5.01) cortices estimated with PET (Table 1).

DISCUSSION

We presented the synthesis and evaluation of a first M₁ mAChR-selective PET radiotracer, ¹¹C-LSN3172176. The ligand was discovered by Lilly (35,38) in *ex vivo* ligand binding assays using liquid chromatography-mass spectrometry (LC-MS/MS) (57-59). ¹¹C-LSN3172176 was reliably produced in good radiochemical yield, high radiochemical and chemical purity, and in high molar activity, using the palladium catalyzed C-¹¹C Suzuki cross-coupling reaction (49) between ¹¹C-methyl iodide and the 2-oxindolin-6-yl boronic acid precursor.

¹¹C-LSN3172176 displays good pharmacokinetic and imaging characteristics in rhesus monkeys: high brain uptake with peak SUV of 4-9.5 in the striatal and cortical tissues, and low uptake in the cerebellum, brain stem, and pons. TACs were well fitted by the MA1 ($t^*=30$) to produce stable measures of regional V_T : highest in the basal ganglia, frontal cortex, and hippocampus, with low V_T in the cerebellum. PET images are of high quality and tissue kinetics are suitable for an ¹¹C-labeled tracer, with high f_p that can be measured reliably. As predicted from *in-vitro* binding experiments (38), uptake in the monkey brain was seen in all M₁ mAChR rich brain regions similar to the known distribution reported for mouse, rat, and rhesus monkey (3,26,60). High specific binding is also reflected in the BP_{ND} estimates of 4-8.5. Specificity of ¹¹C-LSN3172176 to mAChRs was demonstrated by pretreatment with scopolamine, which reduced ¹¹C-LSN3172176 V_T values to levels indistinguishable from the cerebellum, resulting in 98.5% occupancy. Selectivity for M₁ mAChR was demonstrated by blocking of tracer uptake with the M₁-selective partial agonist AZD6088 in a dose-dependent manner, reducing V_T values across all brain

regions to fairly homogeneous levels upon pre-blocking with 2 mg/kg AZD6088. The lowest V_T was found in the cerebellum and brain stem, with baseline V_T values of 8.1 and 7.7 mL/cm³, respectively. The average V_{ND} value of 6.3 ± 0.8 mL/cm³ derived from the blocking scans is in good agreement with the average baseline V_T in the cerebellum, indicating that cerebellum may be suitable as a reference region for ¹¹C-LSN3172176. This is in line with previous reports that the cerebellum is devoid of mAChRs (51,52). The small difference in cerebellum between baseline and blocking scans is likely attributable to partial volume averaging of cortical uptake into the cerebellum region in the baseline scan. To confirm this, we created a ROI in the inferior portion of the cerebellum and measured the V_T values in control and blocking scans. In this inferior region, we found no difference between baseline V_T (6.3 ± 1.3) and post-blocking V_T (6.8 ± 1.0) values, further supporting the utility of the cerebellum as a reference region.

CONCLUSION

We have carried out the synthesis and pre-clinical evaluation of the novel M₁ mAChR selective radioligand ¹¹C-LSN3172176, and demonstrated its suitability as a PET tracer for quantifying central M₁ mAChR in non-human primates. ¹¹C-LSN3172176 displays high levels of regional uptake and appropriate kinetics in rhesus monkey brain, as well as high regional specific binding signals. Therefore ¹¹C-LSN3172176 was advanced to human for further evaluation.

ACKNOWLEDGEMENT

The authors thank the staff of the Yale PET Center for their expert assistance. Research support was provided by Eli Lilly and Co.

DISCLOSURE

At the time this work was conducted, NK and CJ were employees of Eli Lilly. No other potential conflicts of interest relevant to this article exist.

REFERENCES

1. Thiele A. Muscarinic Signaling in the Brain. *Annu Rev Neurosci.* 2013;36:271-294.
2. Kruse AC, Kobilka BK, Gautam D, Sexton PM, Christopoulos A, Wess J. Muscarinic acetylcholine receptors: novel opportunities for drug development. *Nat Rev Drug Discov.* 2014;13:549-560.
3. Anagnostaras SG, Murphy GG, Hamilton SE, et al. Selective cognitive dysfunction in acetylcholine M1 muscarinic receptor mutant mice. *Nat Neurosci.* 2003;6:51-58.
4. Levey AI. Muscarinic acetylcholine receptor expression in memory circuits: implications for treatment of Alzheimer disease. *Proc Natl Acad Sci U S A.* 1996;93:13541-13546.
5. Levey AI, Edmunds SM, Koliatsos V, Wiley RG, Heilman CJ. Expression of m1-m4 muscarinic acetylcholine receptor proteins in rat hippocampus and regulation by cholinergic innervation. *J Neurosci.* 1995;15:4077-4092.
6. Levey AI, Kitt CA, Simonds WF, Price DL, Brann MR. Identification and localization of muscarinic acetylcholine receptor proteins in brain with subtype-specific antibodies. *J Neurosci.* 1991;11:3218-3226.
7. Serrano-Pozo A, Frosch MP, Masliah E, Hyman BT. Neuropathological alterations in Alzheimer disease. *Cold Spring Harb Perspect Med.* 2011;1:a006189.
8. Wess J, Eglen RM, Gautam D. Muscarinic acetylcholine receptors: mutant mice provide new insights for drug development. *Nat Rev Drug Discov.* 2007;6:721-733.
9. Wess J. Muscarinic acetylcholine receptor knockout mice: novel phenotypes and clinical implications. *Annu Rev Pharmacol Toxicol.* 2004;44:423-450.
10. Shinoe T, Matsui M, Taketo MM, Manabe T. Modulation of synaptic plasticity by physiological activation of M1 muscarinic acetylcholine receptors in the mouse hippocampus. *J Neurosci.* 2005;25:11194-11200.
11. Nathan PJ, Watson J, Lund J, et al. The potent M1 receptor allosteric agonist GSK1034702 improves episodic memory in humans in the nicotine abstinence model of cognitive dysfunction. *Int J Neuropsychopharmacol.* 2013;16:721-731.
12. van der Zee EA, Luiten PG. Muscarinic acetylcholine receptors in the hippocampus, neocortex and amygdala: a review of immunocytochemical localization in relation to learning and memory. *Prog Neurobiol.* 1999;58:409-471.

13. Foster DJ, Choi DL, Conn PJ, Rook JM. Activation of M1 and M4 muscarinic receptors as potential treatments for Alzheimer's disease and schizophrenia. *Neuropsychiatr Dis Treat*. 2014;10:183-191.
14. Lebois EP, Schroeder JP, Esparza TJ, et al. Disease-modifying effects of M1 muscarinic acetylcholine receptor activation in an Alzheimer's disease mouse model. *ACS Chem Neurosci*. 2017;8:1177-1187.
15. Ma L, Seager MA, Wittmann M, et al. Selective activation of the M1 muscarinic acetylcholine receptor achieved by allosteric potentiation. *Proc Natl Acad Sci U S A*. 2009;106:15950-15955.
16. Jiang S, Li Y, Zhang C, et al. M1 muscarinic acetylcholine receptor in Alzheimer's disease. *Neurosci Bull*. 2014;30:295-307.
17. Scarr E. Muscarinic M1 receptor agonists: can they improve cognitive performance? *Int J Neuropsychopharmacol*. 2013;16:717-720.
18. Carruthers SP, Gurvich CT, Rossell SL. The muscarinic system, cognition and schizophrenia. *Neurosci Biobehav Rev*. 2015;55:393-402.
19. Hatcher JP, Loudon JM, Hagan JJ, Clark MS. Sabcomeline (SB-202026), a functionally selective M1 receptor partial agonist, reverses delay-induced deficits in the T-maze. *Psychopharmacology (Berl)*. 1998;138:275-282.
20. Wienrich M, Meier D, Ensinger HA, et al. Pharmacodynamic profile of the M1 agonist talsaclidine in animals and man. *Life Sci*. 2001;68:2593-2600.
21. Caccamo A, Fisher A, LaFerla FM. M1 agonists as a potential disease-modifying therapy for Alzheimer's disease. *Curr Alzheimer Res*. 2009;6:112-117.
22. Sellin AK, Shad M, Tamminga C. Muscarinic agonists for the treatment of cognition in schizophrenia. *CNS Spectr*. 2008;13:985-996.
23. Fisher A. M1 muscarinic agonists target major hallmarks of Alzheimer's disease--an update. *Curr Alzheimer Res*. 2007;4:577-580.
24. Fisher A. M1 muscarinic agonists target major hallmarks of Alzheimer's disease--the pivotal role of brain M1 receptors. *Neurodegener Dis*. 2008;5:237-240.

25. Felder CC, Goldsmith PJ, Jackson K, et al. Current status of muscarinic M1 and M4 receptors as drug targets for neurodegenerative diseases. *Neuropharmacology*. 2018.
26. Vora MM, Finn RD, Boothe TE, Liskowsky DR, Potter LT. [N-methyl-¹¹C]-scopolamine: synthesis and distribution in rat brain. *J Labelled Comp Radiopharm*. 1983;20:1229-1236.
27. Mulholland GK, Kilbourn MR, Sherman P, et al. Synthesis, in vivo biodistribution and dosimetry of [¹¹C]N-methylpiperidyl benzilate ([¹¹C]NMPB), a muscarinic acetylcholine receptor antagonist. *Nucl Med Biol*. 1995;22:13-17.
28. Dewey SL, Macgregor RR, Brodie JD, et al. Mapping muscarinic receptors in human and baboon brain using [N-¹¹C-methyl]-benztropine. *Synapse*. 1990;5:213-223.
29. Varastet M, Brouillet E, Chavoix C, et al. In vivo visualization of central muscarinic receptors using [¹¹C]quinuclidinyl benzilate and positron emission tomography in baboons. *Eur J Pharmacol*. 1992;213:275-284.
30. Farde L, Suhara T, Halldin C, et al. PET study of the M1-agonists [¹¹C]xanomeline and [¹¹C]butylthio-TZTP in monkey and man. *Dementia*. 1996;7:187-195.
31. Ridler K, Cunningham V, Huiban M, et al. An evaluation of the brain distribution of [(¹¹C)GSK1034702, a muscarinic-1 (M1) positive allosteric modulator in the living human brain using positron emission tomography. *EJNMMI Res*. 2014;4:66.
32. Buitter HJ, Windhorst AD, Huisman MC, et al. [¹¹C]AF150(S), an agonist PET ligand for M1 muscarinic acetylcholine receptors. *EJNMMI Res*. 2013;3:19.
33. Buitter HJC, Leysen JE, Schuit RC, Fisher A, Lammertsma AA, Windhorst AD. Radiosynthesis and biological evaluation of the M1 muscarinic acetylcholine receptor agonist ligand [¹¹C]AF150(S). *J Labelled Comp Radiopharm*. 2012;55:264-273.
34. Malmquist J, Varnas K, Svedberg M, et al. Discovery of a Novel Muscarinic Receptor PET Radioligand with Rapid Kinetics in the Monkey Brain. *ACS Chem Neurosci*. 2018;9:224-229.
35. Jesudason C, Barth V, Goldsmith P, et al. Discovery of two novel, selective agonist radioligands as PET imaging agents for the M1 muscarinic acetylcholine receptor [abstract]. *J Nucl Med*. 2017;58:546.
36. Nabulsi N, Holden D, Zheng M-Q, et al. Evaluation of a novel, selective M1 muscarinic acetylcholine receptor ligand ¹¹C-LSN3172176 in non-human primates [abstract]. *J Nucl Med*. 2017;58:275.

- 37.** Takai K, Sumiyoshi T, Suwa A, Takahashi Y, Uruno Y, Murata Y, et al. Preparation of fused-ring pyrrolidine derivatives as selective M1 and M4 muscarinic receptor agonists. US patent WO2012020813A1, 2012.
- 38.** Mogg AJ, Eessalu T, Johnson M, et al. In vitro pharmacological characterization and in vivo validation of LSN3172176 a novel M1 selective muscarinic receptor agonist tracer molecule for positron emission tomography. *JPET*. 2018;365:602-613.
- 39.** Nabulsi NB, Mercier J, Holden D, et al. Synthesis and preclinical evaluation of ¹¹C-UCB-J as a PET tracer for imaging the synaptic vesicle glycoprotein 2A in the brain. *J Nucl Med*. 2016;57:777-784.
- 40.** Sandiego CM, Weinzimmer D, Carson RE. Optimization of PET-MR registrations for nonhuman primates using mutual information measures: a multi-transform method (MTM). *Neuroimage*. 2013;64:571-581.
- 41.** Hilton J, Yokoi F, Dannals RF, Ravert HT, Szabo Z, Wong DF. Column-switching HPLC for the analysis of plasma in PET imaging studies. *Nucl Med Biol*. 2000;27:627-630.
- 42.** Wilson AA, Jin L, Garcia A, DaSilva JN, Houle S. An admonition when measuring the lipophilicity of radiotracers using counting techniques. *Appl Radiat Isot*. 2001;54:203-208.
- 43.** Ichise M, Toyama H, Innis RB, Carson RE. Strategies to improve neuroreceptor parameter estimation by linear regression analysis. *J Cereb Blood Flow Metab*. 2002;22:1271-1281.
- 44.** Innis RB, Cunningham VJ, Delforge J, et al. Consensus nomenclature for in vivo imaging of reversibly binding radioligands. *J Cereb Blood Flow Metab*. 2007;27:1533-1539.
- 45.** Lammertsma AA, Hume SP. Simplified reference tissue model for PET receptor studies. *Neuroimage*. 1996;4:153-158.
- 46.** Cunningham VJ, Rabiner EA, Slifstein M, Laruelle M, Gunn RN. Measuring drug occupancy in the absence of a reference region: the Lassen plot re-visited. *J Cereb Blood Flow Metab*. 2010;30:46-50.
- 47.** Larsen P, Ulin J, Dahlstrøm K, Jensen M. Synthesis of [¹¹C]iodomethane by iodination of [¹¹C]methane. *Appl Radiat Isot*. 1997;48:153-157.
- 48.** Andersson Y, Cheng AP, Langstrom B. Palladium-promoted coupling reactions of [¹¹C]methyl iodide with organotin and organoboron compounds. *Acta Chem Scand*. 1995;49:683-688.

49. Suzuki M, Doi H, Koyama H, et al. Pd0-mediated rapid cross-coupling reactions, the rapid C-[11C]methylations, revolutionarily advancing the syntheses of short-lived PET molecular probes. *Chem Rec.* 2014;14:516-541.
50. Waterhouse RN. Determination of lipophilicity and its use as a predictor of blood-brain barrier penetration of molecular imaging agents. *Mol Imaging Biol.* 2003;5:376-389.
51. Enna SJ, Bennett JP, Jr., Bylund DB, et al. Neurotransmitter receptor binding: regional distribution in human brain. *J Neurochem.* 1977;28:233-236.
52. Mash DC, Potter LT. Autoradiographic localization of M1 and M2 muscarine receptors in the rat brain. *Neuroscience.* 1986;19:551-564.
53. Cortes R, Probst A, Tobler HJ, Palacios JM. Muscarinic cholinergic receptor subtypes in the human brain. II. Quantitative autoradiographic studies. *Brain Res.* 1986;362:239-253.
54. Bromberg-Martin ES, Matsumoto M, Hikosaka O. Dopamine in motivational control: rewarding, aversive, and alerting. *Neuron.* 2010;68:815-834.
55. Rinaldi A, Oliverio A, Mele A. Spatial memory, plasticity and nucleus accumbens. *Rev Neurosci.* 2012;23:527-541.
56. Parsey RV, Slifstein M, Hwang DR, et al. Validation and reproducibility of measurement of 5-HT1A receptor parameters with [carbonyl-11C]WAY-100635 in humans: comparison of arterial and reference tissue input functions. *J Cereb Blood Flow Metab.* 2000;20:1111-1133.
57. Barth V, Need A. Identifying novel radiotracers for PET imaging of the brain: application of LC-MS/MS to tracer identification. *ACS Chem Neurosci.* 2014;5:1148-1153.
58. Need A, Kant N, Jesudason C, Barth V. Approaches for the discovery of novel positron emission tomography radiotracers for brain imaging. *Clin Transl Imaging.* 2017;5:265-274.
59. Jesudason CD, DuBois S, Johnson M, Barth VN, Need AB. In vivo receptor occupancy in rodents by LC-MS/MS. In: Sittampalam GS, Coussens NP, Brimacombe K, et al., eds. *Assay Guidance Manual.* Bethesda (MD); 2004.
60. Yamamura HI, Kuhar MJ, Greenberg D, Snyder SH. Muscarinic cholinergic receptor binding: regional distribution in monkey brain. *Brain Res.* 1974;66:541-546.

FIGURES AND TABLES

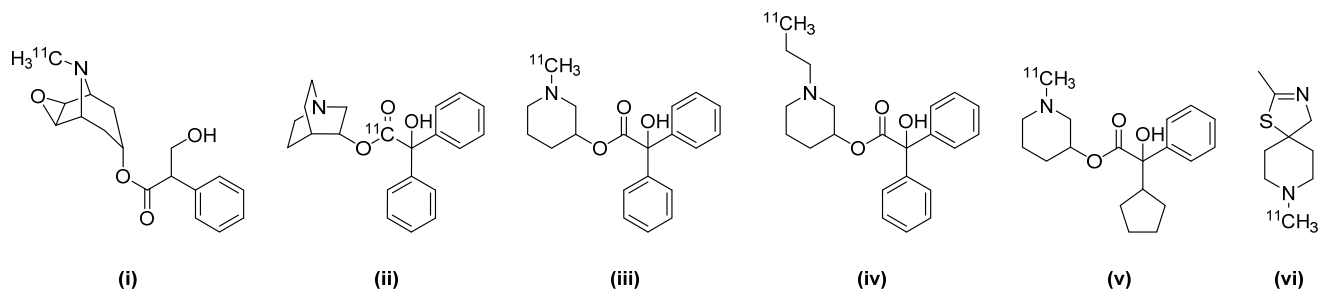


FIGURE 1: Chemical structures of reported PET tracers for the muscarinic acetylcholine receptors: (i) ^{11}C -scopolamine; (ii) ^{11}C -QNB; (iii) ^{11}C -MPB; (iv) ^{11}C -PPB; (v) (*S*)-1-(methyl- ^{11}C)piperidin-3-yl (*R*)-2-cyclopentyl-2-hydroxy-2-phenylacetate; (vi) ^{11}C -AF150(S).

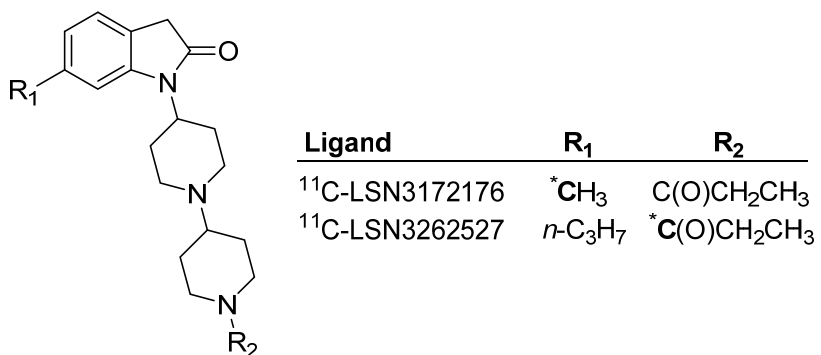


FIGURE 2. Novel selective agonist for M1 muscarinic acetylcholine receptor. The boldface letter C with asterisk indicates ¹¹C-radiolabeling site.

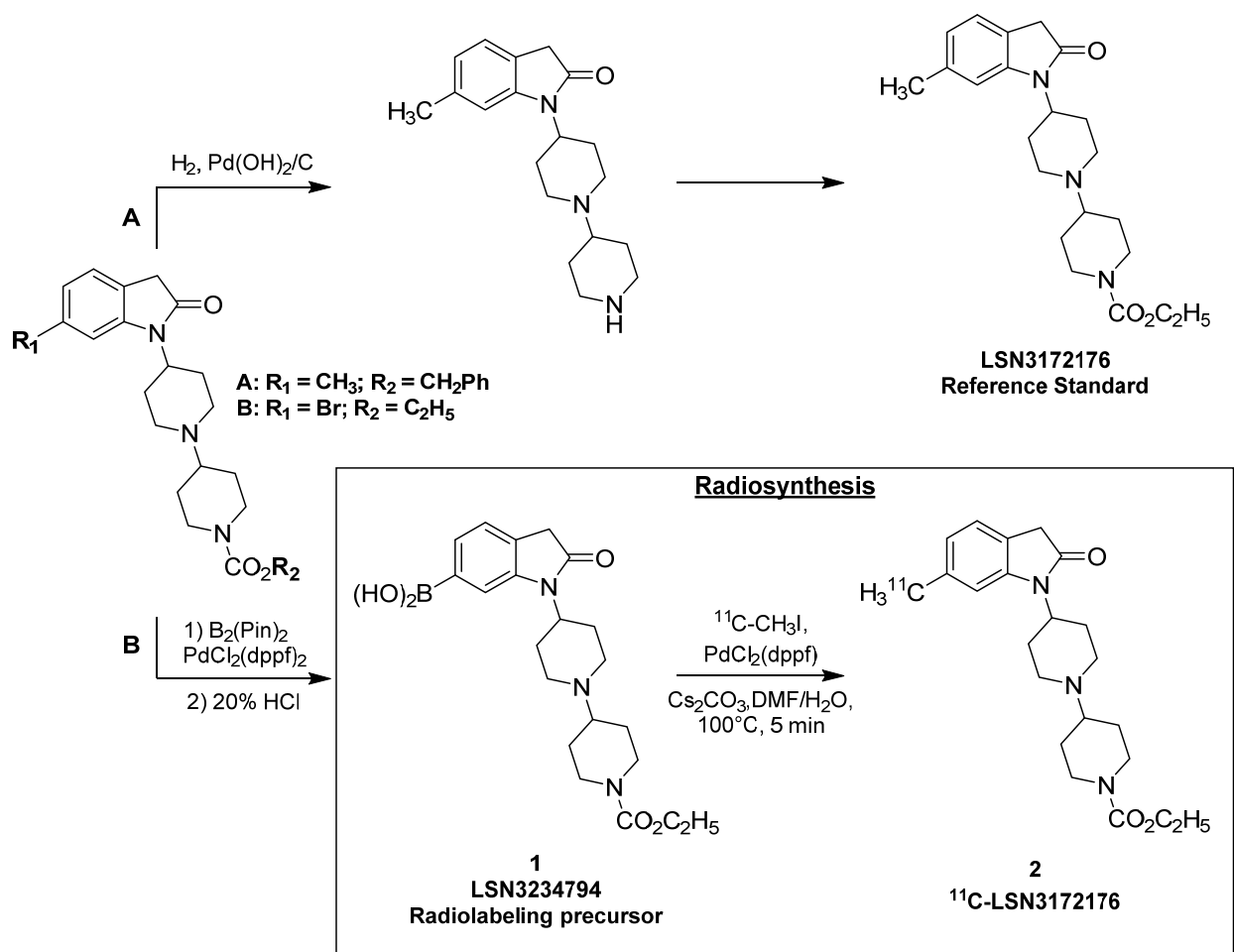


FIGURE 3. Brief scheme outlining the synthesis of LSN3172176 and the radiolabeling precursor, as well as the radiosynthesis of ^{11}C -LSN3172176.

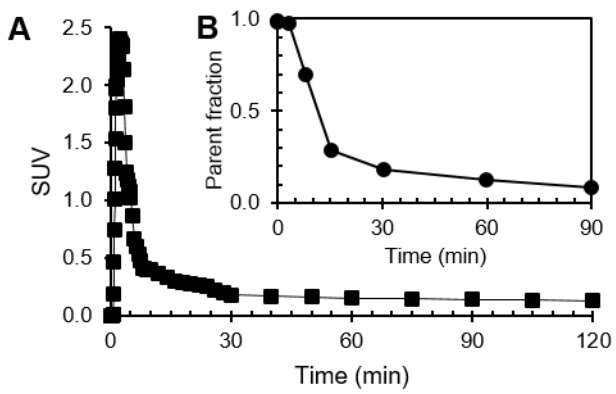


FIGURE 4. Metabolite-corrected plasma activity (A) and parent fraction in plasma (B) over time for ¹¹C-LSN3172176.

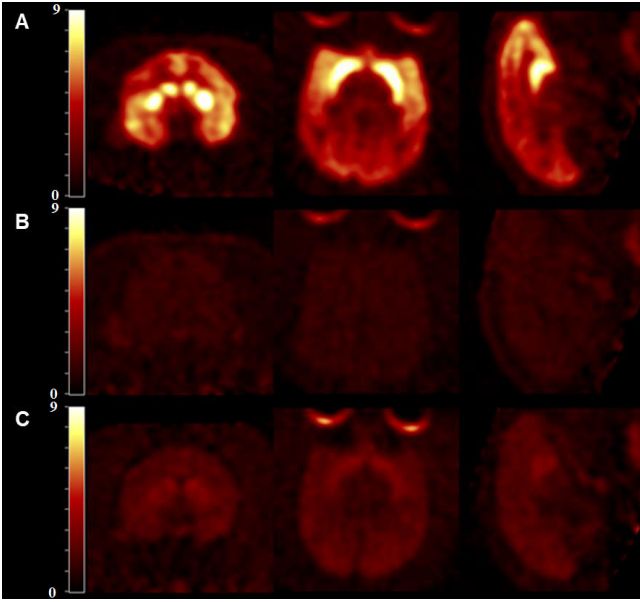


FIGURE 5. Representative PET SUV images summed from 30-45 min after ^{11}C -LSN3172176 injection from: A. a baseline scan; B. after pretreatment with scopolamine (50 µg/kg); C. after pretreatment with AZD6088 (2 mg/kg).

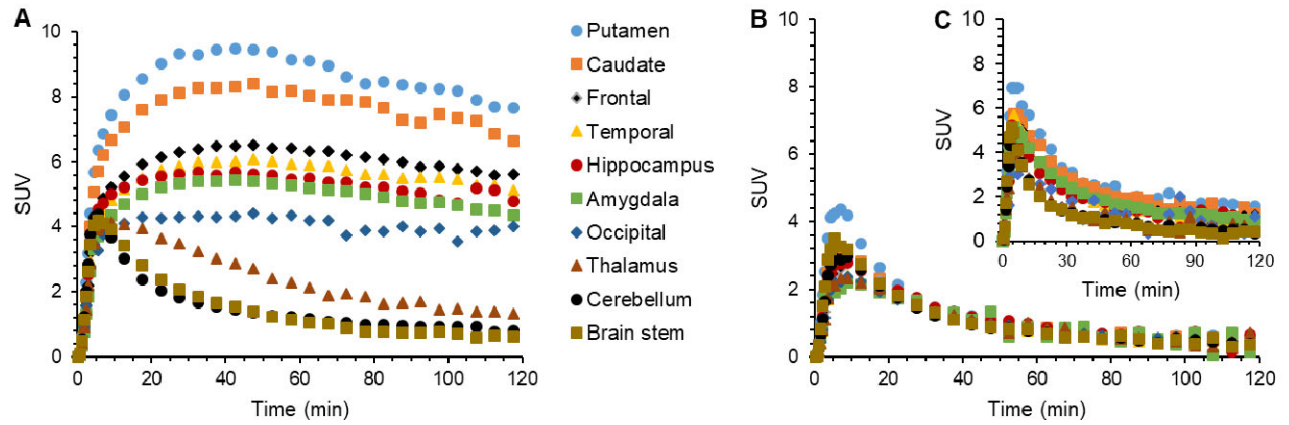


FIGURE 6. Representative time – activity curves in selected brain regions from ¹¹C-LSN3172176 baseline (A) and blocking scans after pretreatment with scopolamine (50 µg/kg) (B), and with 2 mg AZD6088 (2 mg/kg) (C).

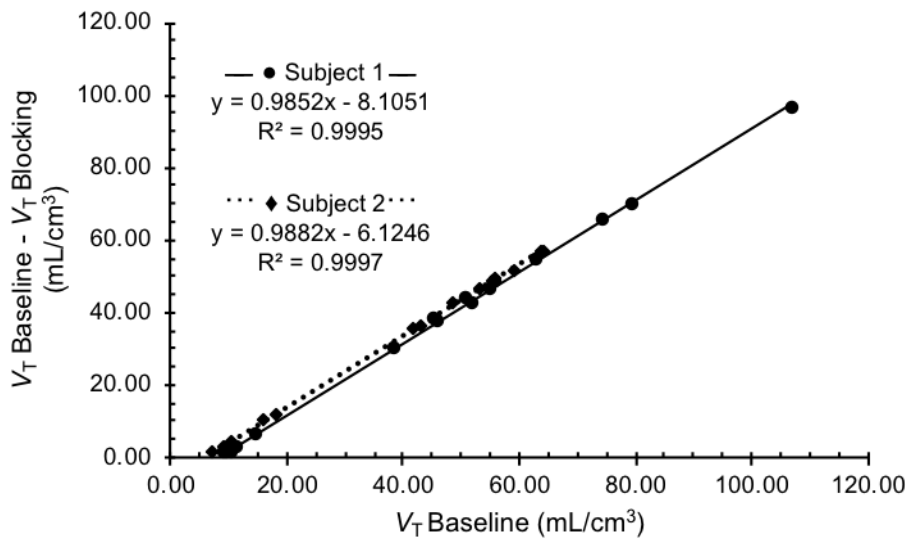


FIGURE 7. Regional V_T values for ^{11}C -LSN3172176 preblocking scans with scopolamine (50 $\mu\text{g}/\text{kg}$, $n=2$).

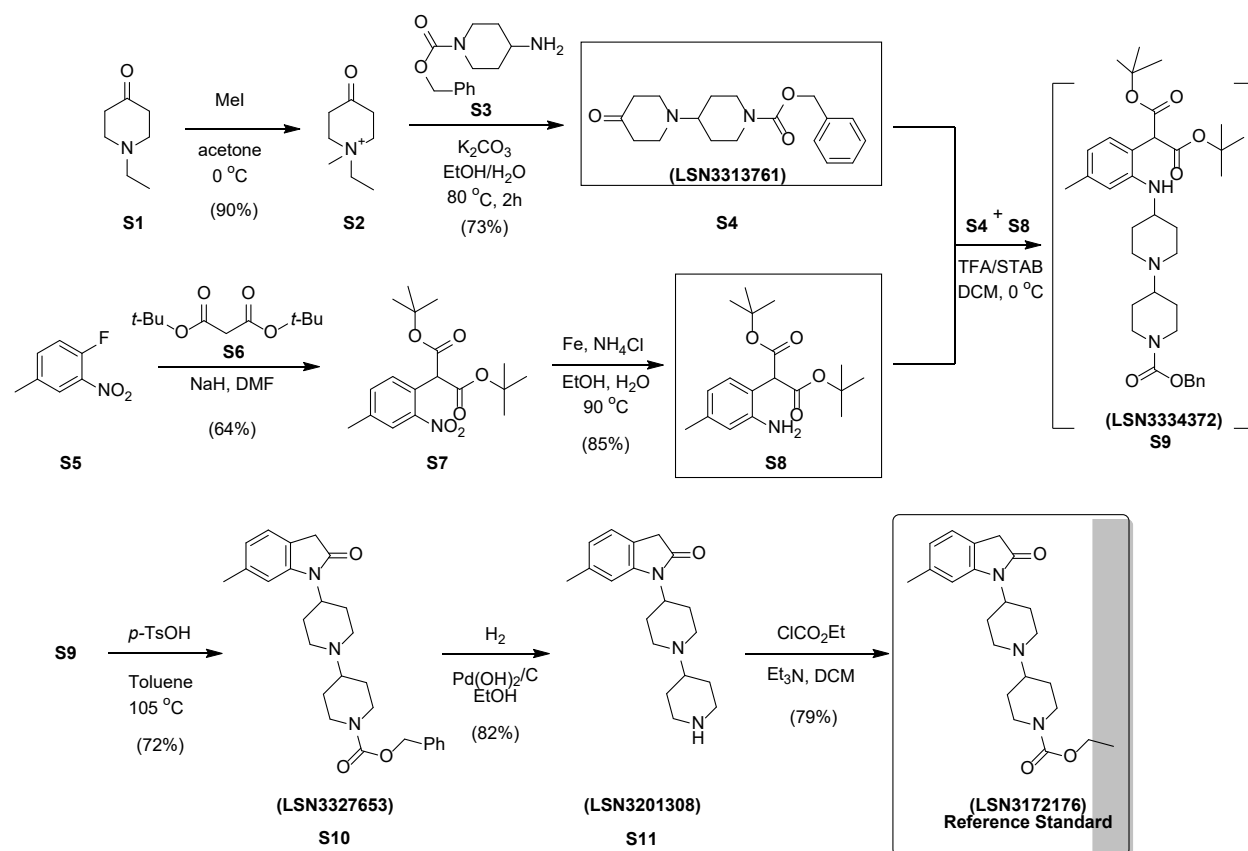
Brain region	Preblocking V_T (MA1, $t^* = 30$)				BP_{ND}	
	Baseline V_T ($n = 4$)	Scopolamine	AZD6088		SRTM	MA1 ($t^* = 30$)
		50 μ g/kg ($n = 2$)	0.67 mg/kg ($n = 1$)	2 mg/kg ($n = 1$)	Baseline ($n = 4$)	Baseline ($n = 4$)
Amygdala	33.8 (4.0)	7.2 (1.3)	13.49	8.40	2.54 (0.3)	3.23 (0.54)
Brain stem	7.7 (0.9)	7.3 (1.1)	7.28	5.99	0.08 (0.02)	-0.04 (0.07)
Caudate	62.6 (10)	8.0 (1.0)	24.29	13.83	5.46 (0.62)	6.77 (0.76)
Cerebellum	8.1 (1.3)	7.0 (1.2)	7.37	6.41	--	--
Cingulate	53.8 (7.1)	8.1 (0.8)	19.55	12.12	4.45 (0.2)	5.68 (0.26)
Frontal cortex	50.7 (5)	7.5 (0.5)	17.92	11.25	4.03 (0.2)	5.33 (0.37)
Globus pallidus	27.4 (2.6)	7.8 (1.3)	15.59	9.14	2.09 (0.14)	2.42 (0.21)
Hippocampus	43.5 (6.0)	8.0 (1.3)	18.16	10.19	3.37 (0.31)	4.41 (0.51)
Insula	56.6 (7.9)	7.8 (1.1)	18.50	11.65	4.56 (0.31)	6.02 (0.38)
Nucleus accumbens	75.6 (4.7)	8.2 (1.3)	30.33	12.82	6.24 (0.44)	8.48 (0.85)
Occipital cortex	40.4 (5.2)	7.1 (0.9)	18.11	11.54	3.08 (0.13)	4.02 (0.18)
Pons	8.5 (1.1)	8.1 (0.9)	8.26	7.06	0.17 (0.04)	0.05 (0.06)
Putamen	68.6 (10.7)	8.8 (2.0)	26.67	15.85	6.04 (0.59)	7.50 (0.6)
Substantia nigra	10.3 (1.8)	7.7 (1.3)	8.55	10.57	0.37 (0.05)	0.27 (0.07)
Temporal cortex	48.5 (6.9)	6.8 (0.7)	17.76	11.00	3.77 (0.18)	5.01 (0.22)
Thalamus	13.6 (1.7)	7.0 (1.1)	10.75	7.11	0.75 (0.12)	0.69 (0.14)

TABLE 1. Regional binding parameters for ^{11}C -LSN3172176 at baseline and after preblocking with scopolamine and AZD6088. Values in parenthesis are standard deviations.

Chemistry

I. Synthesis of LSN3172176 reference standard:

Supplemental Scheme 1



1-Ethyl-1-methyl-4-oxopiperidin-1-ium iodide (S2). Methyl iodide (150 g, 1056.8 mmol) was added dropwise to a solution of 1-ethylpiperidin-4-one (**S1**, 100 g, 786.3 mmol) in acetone (1 L) cooled at 0 °C. The mixture was let warm to room temperature (r.t.) and stirred for 18 h. The solids were filtered, rinsed with acetone (300 mL), and dried under vacuum at ~50°C to give **S2** (201 g, 90%) as a white solid. ¹H NMR (399.83 MHz, DMSO): 3.70 (t, *J* = 6.6 Hz, 4H), 3.55 (q, *J* = 7.3 Hz, 2H), 3.15 (s, 3H), 2.76-2.62 (m, 4H), 1.28 (t, *J* = 7.3 Hz, 3H).

Benzyl 4-oxo-[1,4'-bipiperidine]-1'-carboxylate (S4). A solution of 4-amino-1-*N*-Cbz-piperidine (**S3**, 3g, 12.4 mmol) and potassium carbonate (5.2 g, 37.2 mmol) in a mixture of EtOH (15 mL) and water (10 mL) was treated with **S2** (4.0 g, 14.9 mmol). The reaction mixture was heated at 80 °C for 18 h. After cooling

to r.t. the mixture was poured into water (50 mL) and extracted with CH₂Cl₂ (3 × 50 mL). The combined organic phase was dried over anhydrous MgSO₄, filtered, and concentrated under vacuum. The crude product was purified by silica gel column chromatography (40g), eluting with a gradient 0-30% [4:1 EtOAc:MeOH]/CH₂Cl₂ to give **S4** as a solid (30.03 g, 73%). ¹H NMR (400.13 MHz, CDCl₃): 7.39-7.36 (m, 5H), 5.15 (s, 2H), 4.37-4.30 (m, 2H), 2.88-2.79 (m, 5H), 2.75-2.74 (m, 1H), 2.47 (t, *J* = 5.7 Hz, 4H), 1.88-1.77 (m, 2H), 1.60 (s, 2H), 1.57-1.51 (m, 1H).

Di-tert-butyl 2-(4-methyl-2-nitrophenyl)malonate (S7). A solution of di-tert-butyl malonate (**S6**) (6.51 mL, 29.00 mmol) in DMF (30 mL) was treated at r.t. with sodium hydride (1.16 g, 29.00 mmol) and the mixture stirred for 40 min. Then, 1-fluoro-4-methyl-2-nitro-benzene (**S5**, 3.0 g, 19.33 mmol) was added and the reaction mixture was stirred at r.t. for 18 h. The mixture was partitioned between EtOAc (100 mL) and 5% aqueous LiCl (100 mL). The organic layer was washed with brine (3 × 100 mL), dried over anhydrous Na₂SO₄, filtered, and concentrated to dryness. The crude product was purified by silica gel column chromatography (0-10% EtOAc in hexanes) to give **S7** (4.33 g, 64%) as a white solid. ¹H NMR (399.83 MHz, CDCl₃): 7.83 (m, 1H), 7.42 (m, 2H), 5.05 (s, 1H), 2.42 (s, 3H), 1.48 (s, 18H).

Di-tert-butyl 2-(2-amino-4-methylphenyl)malonate (S8). A stirred slurry of **S7** (4.33 g, 12.3 mmol), Fe (2.06 g, 37.0 mmol), and ammonium chloride (3.30 g, 61.6 mmol) in EtOH (26 mL) and water (10 mL) was heated at 90 °C for 1.5 h. The mixture was concentrated under vacuum and the residue filtered through a pad of celite eluting with CH₂Cl₂. The resulting solution was concentrated and purified by silica gel column chromatography (10-20% EtOAc in hexanes) to give **S8** (3.96 g, 85%) as a light orange oil. ¹H NMR (399.83 MHz, CDCl₃): 7.04 (d, *J* = 7.7 Hz, 1H), 6.59-6.55 (m, 2H), 4.42 (s, 1H), 2.23 (s, 3H), 1.46 (s, 18H).

Di-tert-butyl 2-(2-((1'-((benzyloxy)carbonyl)-[1,4'-bipiperidin]-4-yl)amino)-4-methylphenyl)malonate (S9). A solution of **S8** (12.01 g, 37.37 mmol) and **S4** (13.01 g, 41.12 mmol) in CH₂Cl₂ (200 mL), cooled at 0 °C, was treated with trifluoroacetic acid (7 mL, 92.58 mmol), followed by portion-wise addition of sodium triacetoxyborohydride (STAB; 15.84 g, 74.74 mmol). The mixture was then allowed to warm to r.t. overnight. A saturated aqueous solution of NaHCO₃ (150 mL) was added and the aqueous layer was

extracted with CH_2Cl_2 (2×100 mL). The combined organic phase was dried over anhydrous Na_2SO_4 , filtered, and concentrated to give **S9** as a brown oil, which was used in the next step without further purification. ^1H NMR (400.13 MHz, DMSO): 7.38-7.32 (m, 6H), 6.92 (d, $J=7.7$ Hz, 1H), 6.47 (s, 1H), 6.41 (d, $J=7.8$ Hz, 1H), 5.07 (s, 2H), 4.75 (s, 1H), 4.72-4.66 (m, 1H), 4.08-4.02 (m, 2H), 3.91 (s, 3H), 3.32 (s, 3H), 3.29-3.27 (m, 1H), 2.90-2.82 (m, 4H), 2.40-2.38 (m, 2H), 2.21-2.19 (m, 4H), 1.91-1.86 (m, 2H), 1.79-1.69 (m, 2H), 1.42 (s, 24H).

Benzyl 4-(6-methyl-2-oxoindolin-1-yl)-[1,4'-bipiperidine]-1'-carboxylate (S10). A solution of **S9** (23.24 g, 37.38 mmol) and *p*-toluenesulfonic acid (9.00 g, 52.26 mmol) in toluene (500 mL) was heated overnight at 105 °C. The reaction mixture was cooled to r.t. and the solvent was removed under vacuum. The residue was partitioned between a saturated aqueous solution of NaHCO_3 (200 mL) and CH_2Cl_2 (200 mL). The aqueous phase was extracted with CH_2Cl_2 (2×100 mL). The combined organic phase was dried over Na_2SO_4 , filtered, and concentrated under reduced pressure. The crude product was purified by column chromatography with silica gel (260 g) eluting with EtOAc in Hexanes (40-64% gradient) to give **S10** (12.06 g, 72%) as a tan solid. ^1H NMR (400.13 MHz, DMSO): 7.37 (s, 5H), 7.13-7.11 (m, 1H), 6.95 (s, 1H), 6.80-6.78 (m, 1H), 5.08 (s, 2H), 4.06 (d, $J=10.7$ Hz, 3H), 3.46 (s, 2H), 3.33 (d, $J=1.6$ Hz, 3H), 2.95-2.89 (m, 4H), 2.32 (s, 7H), 1.77-1.75 (m, 2H), 1.56 (s, 2H), 1.36-1.34 (m, 2H).

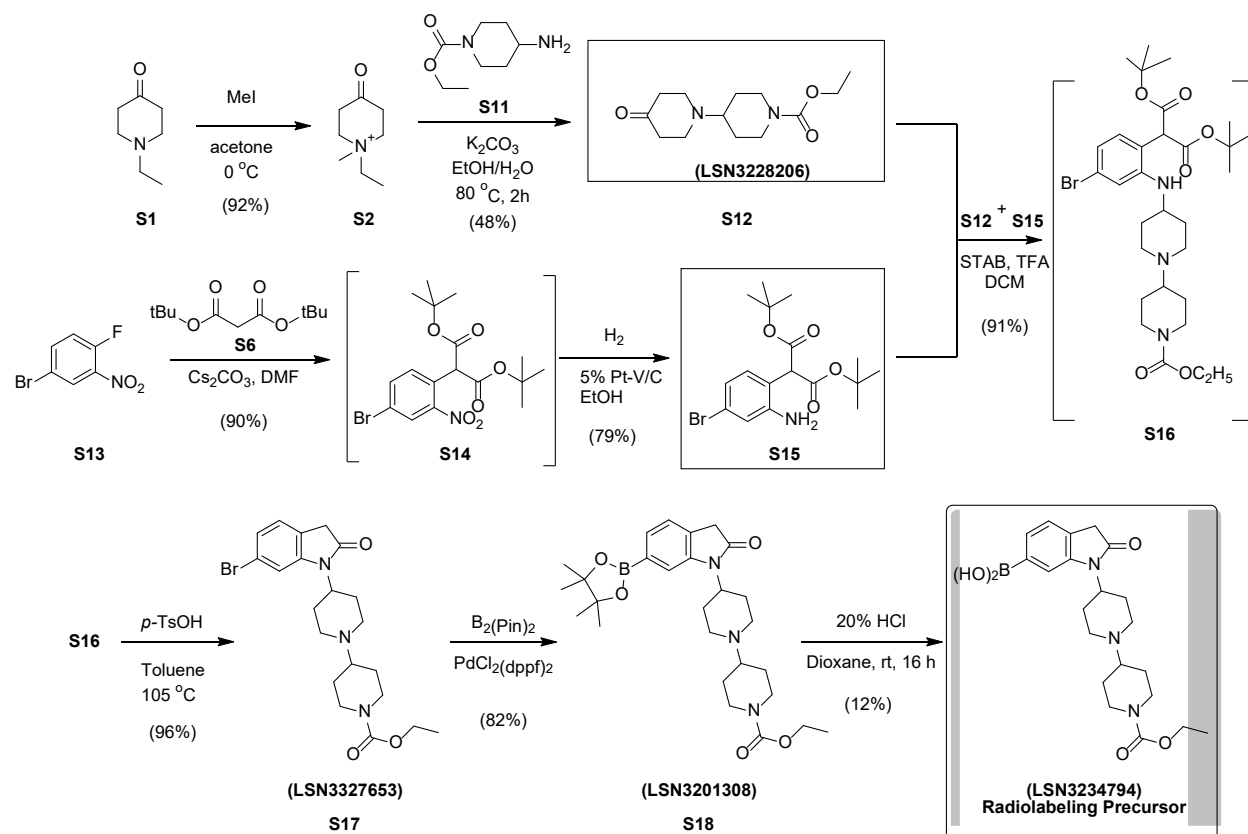
1-([1,4'-bipiperidin]-4-yl)-6-methylindolin-2-one (S11). To a solution of **S10** (12.06 g, 26.9 mmol) in EtOH (250 mL) was added to a slurry of 20% $\text{Pd}(\text{OH})_2/\text{C}$ in EtOH (250 mL) that was previously purged under a stream of nitrogen. Then, the reaction mixture was sealed, pressurized with hydrogen (60 psi) and agitated for 2 h at r.t. The mixture was filtered through a pad of Celite and the solution concentrated under vacuum yielding **S11** (6.92 g, 82%) as a tan solid. ^1H NMR (400.13 MHz, DMSO): 8.82-8.81 (m, 1H), 7.12 (d, $J=7.4$ Hz, 1H), 6.95 (s, 1H), 6.80 (d, $J=7.5$ Hz, 1H), 4.06-4.00 (m, 1H), 3.25 (d, $J=12.6$ Hz, 2H), 2.95 (d, $J=8.6$ Hz, 2H), 2.80 (dd, $J=10.4, 12.3$ Hz, 2H), 2.60-2.55 (m, 1H), 2.32-2.29 (m, 7H), 1.86 (d, $J=11.8$ Hz, 2H), 1.72-1.58 (m, 4H).

Ethyl 4-(6-methyl-2-oxoindolin-1-yl)-[1,4'-bipiperidine]-1'-carboxylate (LSN3172176). A solution of **S11** (6.92 g, 22.1 mmol) and triethylamine (4.0 mL, 28.7 mmol) in CH_2Cl_2 (250 mL) was cooled at 0 °C

and treated dropwise with ethyl chloroformate (2.56 mL, 26.5 mmol). The reaction was allowed to warm to r.t. overnight. A saturated aqueous solution of NaHCO₃ (100 mL) was added to the reaction mixture. After decanting, the aqueous phase was extracted with CH₂Cl₂ (2 × 50 mL). The combined organic phase was dried over Na₂SO₄ and concentrated under vacuum. The resulting brown oil was purified by silica gel chromatography (20% CH₂Cl₂ in EtOH) to give LSN3172176 (6.72 g, 79%) as a white solid. ¹H NMR (400.13 MHz, DMSO): 7.11 (d, *J* = 7.4 Hz, 1H), 6.94 (s, 1H), 6.79 (d, *J* = 7.4 Hz, 1H), 4.02 (q, *J* = 7.0 Hz, 5H), 3.45 (s, 2H), 3.32 (s, 3H), 2.95 (d, *J* = 8.1 Hz, 2H), 2.86-2.79 (m, 2H), 2.51-2.50 (m, 5H), 2.32-2.28 (m, 7H), 1.74 (d, *J* = 11.7 Hz, 2H), 1.57 (d, *J* = 9.3 Hz, 2H), 1.33 (qd, *J* = 12.1, 3.9 Hz, 2H), 1.17 (t, *J* = 7.1 Hz, 3H). ¹³C NMR (100.61 MHz, DMSO): 174.5, 154.5, 143.9, 136.8, 124.1, 121.8, 121.8, 110.0, 61.4, 60.9, 50.2, 48.4, 43.0, 35.1, 28.2, 27.6, 21.4, 14.6; HRMS (ESI) calcd for C₂₂H₃₂N₃O₃ [M + H]⁺ 386.24, found 386.24.

II. Synthesis of the radiolabeling precursor LSN3234794:

Supplemental Scheme 2



Ethyl 4-oxo-[1,4'-bipiperidine]-1'-carboxylate (S12). Potassium carbonate (174 g, 1,260.9 mmol) was added to a solution of 1-ethyl-1-methyl-4-oxopiperidin-1-ium iodide (S2, 200 g, 743.2 mmol) and ethyl 4-aminopiperidine-1-carboxylate (S11, 108 g, 627.1 mmol) in EtOH (1,500 mL) and water (900 mL) at r.t. The mixture was heated to 80 °C for 2 h, then cooled to room temperature and ethanol was removed at 45-50 °C. The residual solution was extracted with CH₂Cl₂ (3 × 500 mL) and the combined organic phase was washed with water (1 L) and concentrated under vacuum. The crude mixture was purified by silica gel column chromatography (eluent: MeOH/CH₂Cl₂ (0:1 to 1:5)) to give S12 as a brown oil (77.0 g, 48.3%). ¹H NMR (400.13 MHz, DMSO): 4.02 (q, *J* = 7.0 Hz, 4H), 2.78 (t, *J* = 5.9 Hz, 6H), 2.69-2.61 (m, 1H), 2.31 (t, *J* = 5.8 Hz, 4H), 1.74 (d, *J* = 12.2 Hz, 2H), 1.38-1.24 (m, 2H), 1.18 (t, *J* = 7.1 Hz, 3H).

Di-*tert*-butyl 2-(4-bromo-2-nitrophenyl)malonate (S14). A solution of di-*tert*-butyl malonate (118 g, 545.6 mmol) in DMF (1 L) was treated with cesium carbonate (370 g, 1135.6 mmol) and the mixture was stirred at r.t. for 20 min. Then 4-bromo-1-fluoro-2-nitrobenzene S13 (100 g, 454.5 mmol) was added and the reaction was left stirring at r.t. for 18 h. The mixture was filtered to remove salts and the solid washed with ethyl acetate (500 mL). The resulting solution was concentrated under reduced pressure at 80 °C. The residue was dissolved in ethyl acetate (500 mL) and washed with water (500 mL). The organic phase was concentrated under vacuum to give S14 (170.3 g, 90%) as a brown oil, which was used in the next step without further purification. ¹H NMR (399.83 MHz, CDCl₃): 8.14 (d, *J* = 2.0 Hz, 1H), 7.73 (dd, *J* = 2.1, 8.5 Hz, 1H), 7.43 (d, *J* = 8.4 Hz, 1H), 5.02 (s, 1H), 1.46 (s, 18H).

Di-*tert*-butyl 2-(2-amino-4-bromophenyl)malonate (S15). To a solution of S14 (170.3 g, 409.1 mmol) in ethanol (2 L) was added Pt-V/C (20 g). The mixture was purged with argon and then sealed and pressurized to 50 psi with hydrogen. The reaction mixture was stirred at r.t. for 18 h, filtered through a pad of Celite and rinsed with ethanol (500 mL). The solution was concentrated under reduced pressure. The residue was recrystallized from ethanol and heptane to give S15 as a yellow solid (124.8 g, 79%). ¹H NMR (399.83 MHz, CDCl₃): 7.25 (s, 1H), 7.02 (d, *J* = 8.1 Hz, 1H), 6.93-6.90 (m, 2H), 4.40 (s, 1H), 1.46 (s, 18H).

Di-*tert*-butyl 2-(4-bromo-2-((1'-(ethoxycarbonyl)-[1,4'-bipiperidin]-4-yl)amino)phenyl)malonate (S16). To a solution of S15 (102 g, 264.1 mmol) and S12 (75.6 g, 297.25 mmol) in CH₂Cl₂ (1.5 L), cooled

at 0 °C, was added TFA (75 g, 657.7 mmol) followed by STAB (112 g, 528.2 mmol). The reaction was left to warm to r.t. and 7% aqueous NaHCO₃ (1 L) was added slowly while stirring. The mixture was extracted with CH₂Cl₂ (3 × 500 mL) and the combined organic phase was concentrated under vacuum. The crude product was purified by silica gel column chromatography (heptane/EtOAc/TEA, 50:25:1) to give **S16** as a brown oil (150 g, 91%).

Ethyl 4-(6-bromo-2-oxoindolin-1-yl)-[1,4'-bipiperidine]-1'-carboxylate (S17). A solution of **S16** (150 g, 240.1 mmol) and *p*-toluenesulfonic acid monohydrate (63.9 g, 335.9 mmol) in toluene (3 L) was heated at 105 °C for 24 h. The reaction was cooled to r.t., then 7% aqueous NaHCO₃ (1.5 L) was added and the mixture stirred for 20 min. After separation of the phases, the aqueous phase was extracted with CH₂Cl₂ (3 × 1 L). The combined organic phases were concentrated to give **S17** as a pink solid (104 g, 96%). ¹H NMR (400.13 MHz, MeOD): 7.56 (s, 1H), 7.18 (s, 2H), 4.29-4.26 (m, 3H), 4.11 (q, *J* = 7.1 Hz, 2H), 3.14-3.12 (m, 2H), 2.89-2.87 (m, 2H), 2.62-2.57 (m, 5H), 1.94-1.89 (m, 2H), 1.72-1.69 (m, 2H), 1.50-1.40 (m, 2H), 1.26 (t, *J* = 7.1 Hz, 3H).

Ethyl 4-(2-oxo-6-(4,4,5,5-tetramethyl-1,3,2-dioxaborolan-2-yl)indolin-1-yl)-[1,4'-bipiperidine]-1'-carboxylate (S18). A solution of **S17** (104 g, 230.9 mmol), B₂(pin)₂ (130 g, 511.9 mmol), and KOAc (46.4 g, 472.7 mmol) in dioxane (1 L) was purged with nitrogen for 1 h. Then, Pd(dppf)₂-CH₂Cl₂ (18.6 g, 22.8 mmol) was added and the mixture was heated at 50 °C for 15 h. After cooling to r.t., water (1 L) was added. The mixture was extracted with CH₂Cl₂ (4 × 500 mL) and the organic phase concentrated under vacuum. The residue was diluted with methyl *tert*-butyl ether (MTBE; 1 L) and active carbon (10 g) was added. The slurry was heated to 50 °C for 2 h, then cooled to r.t. and filtered through a pad of Celite. The solution was concentrated under vacuum to give an oil, which was used in the next step without further purification.

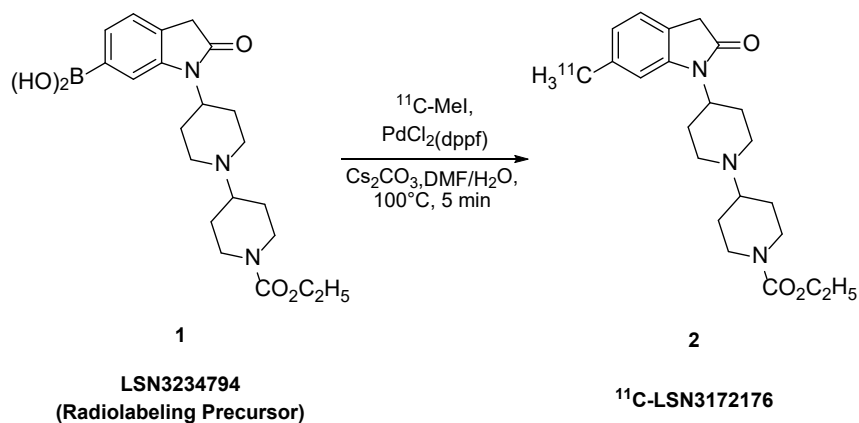
(1-(1'-(ethoxycarbonyl)-[1,4'-bipiperidin]-4-yl)-2-oxoindolin-6-yl)boronic acid (LSN3234794). A solution of **S18** (100 g, 201.0 mmol) in dioxane (300 mL) was treated with 20% aqueous HCl (500 mL), and the mixture was stirred at r.t. for 16 h. Then, 7% aqueous NaHCO₃ was added until pH 8. The resulting solution was extracted with CH₂Cl₂ (3 × 500 mL) and the combined organic phase concentrated under reduced pressure. The crude mixture was dissolved in acetonitrile and water (1:1, 1.6 L) and purified by

preparative HPLC. The fractions containing the product were concentrated under vacuum. The aqueous layer was adjusted to neutral pH with 7% aqueous NaHCO₃ and then extracted with CH₂Cl₂ (3 × 1000 mL). The combined organic phase was concentrated under vacuum to give LSN3234794 (10 g, 12%) as a light yellow solid. ¹H NMR (399.80 MHz, DMSO): 8.12 (s, 2H), 7.51 (s, 1H), 7.45 (d, *J* = 7.3 Hz, 1H), 7.23 (d, *J* = 7.3 Hz, 1H), 4.03 (q, *J* = 7.1 Hz, 6H), 3.53 (s, 2H), 3.35 (s, 2H), 3.00-2.90 (m, 2H), 2.87-2.61 (m, 2H), 2.47-2.30 (m, 3H), 1.80-1.69 (m, 2H), 1.59-1.49 (m, 2H), 1.47-1.26 (m, 2H), 1.18 (t, *J* = 7.1 Hz, 4H); ¹³C NMR (100 MHz, DMSO): 174.32, 154.68, 143.42, 133.50, 127.89, 127.37, 123.71, 114.39, 61.23, 60.78, 55.09, 50.39, 48.68, 28.27, 27.74, 14.79. HRMS (ESI) calcd for C₂₁H₃₁BN₃O₅ [M + H]⁺ 416.2351, found 416.2677.

Radiochemistry

Synthesis of ¹¹C-LSN3172176 (ethyl 4-(6-(methyl-¹¹C)-2-oxoindolin-1-yl)-[1,4'-bipiperidine]-1'-carboxylate):

Supplemental Scheme 3



The following radio-HPLC systems were used: a preparative HPLC system including a Shimadzu LC-20A pump, a Rheodyne 7133i injector with a 2-mL loop, a Knauer K200 ultraviolet detector, a Bioscan γ -flow detector, and a laptop computer running the EZStart data acquisition software; an analytic HPLC system consisting of a Shimadzu LC-20A quaternary pump, a Rheodyne 7133i injector, a Shimadzu SPD-M20A PDA or SPD-20A ultraviolet detector, a flow cell γ detector (Bioscan), and a PC with Shimadzu Class VP 7.2 software used for system control.

$^{11}\text{CO}_2$ was produced through the $^{14}\text{N}(\text{p},\alpha)^{11}\text{C}$ nuclear reaction by bombardment of a high-pressure target containing a mixture of nitrogen and oxygen (0.5%–1%) with a 16.8-MeV proton beam that was produced by the PETTrace cyclotron (GE Healthcare). ^{11}C -Methyl iodide was synthesized through the gas-phase method from $^{11}\text{CO}_2$ using the FXMeI or the FXC module (GE Healthcare), by converting $^{11}\text{CO}_2$ to ^{11}C -methane, followed by reaction of ^{11}C -methane with iodine at 720 °C (1).

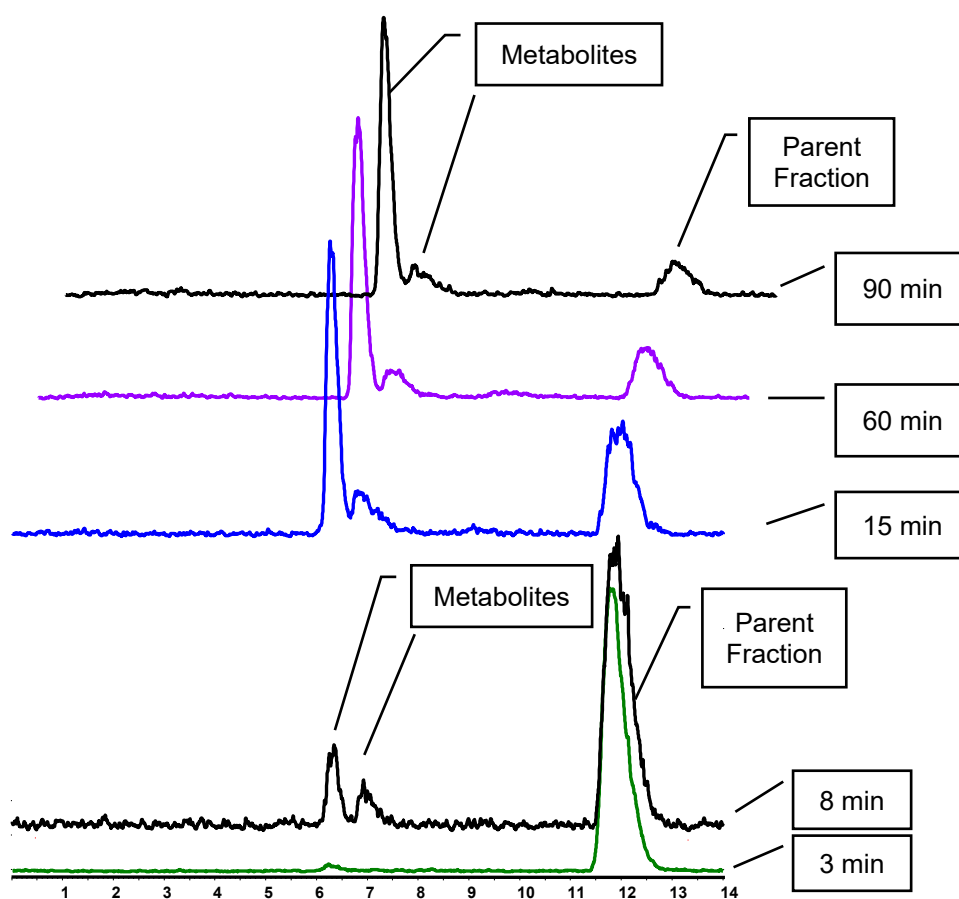
^{11}C -iodomethane was swept with helium through degassed and acetone/ice chilled solution of 0.8-1.2 mg Pd(dppf) $\text{Cl}_2\cdot\text{CH}_2\text{Cl}_2$ and 2-3 mg cesium carbonate in DMF (0.2 mL). After the radioactivity peaked, the mixture was stirred for 2 min at ambient temperature, then a solution of the precursor (1-1.2 mg) in 0.2 mL DMF/water (1:1) was added and the resulting solution was heated for 5 min at 100 °C. After cooling, the solution was diluted with 1.5 mL of the semi-preparative HPLC mobile phase and loaded onto the semi-preparative HPLC column (Gemini C18, 10 μm , 10 \times 250 mm) for purification. The column was eluted at a flow rate of 4 mL/min with 45% acetonitrile/55% of 1:1 mixture of 5 mM ammonium bicarbonate/5 mM ammonium carbonate. The product fraction was collected, diluted with 50 mL of de-ionized (DI) water, and the resulting solution was passed through a Waters C18 Classic SepPak cartridge. The cartridge was rinsed with 10 mL of 0.001 N HCl. The radiolabeled product was recovered by eluting the SepPak with 1 mL of absolute ethanol (USP), followed by 3 mL of saline (USP), and collected into a syringe barrel. Finally the ethanolic saline solution was passed through a sterile 0.22 μm Millex-GV membrane filter for terminal sterilization and collected in an empty sterile vial containing 7 mL of saline (USP) and 40 μL of 4.2% (or 20 μL of 8.4%) sodium bicarbonate (USP) affording a formulated solution ready for dispensing and administration.

Chemical purity, radiochemical purity, and molar activity (A_m) were determined by analytical HPLC (column: Luna C18(2), 4.6 \times 250 mm, 5 μm ; mobile phase: 26% acetonitrile and 74% 0.05 M aqueous ammonium formate with 0.5% acetic acid (v/v, pH 4.2); flow rate: 2 mL/min; UV detector wavelength: 254 nm). The identity of radiolabeled product was confirmed by co-injection with the unlabeled reference standard.

Metabolite Analysis, arterial input function and Log *D* determination

Arterial blood samples were collected at various intervals to measure the plasma input function. In addition, arterial blood samples at 3, 8, 15, 30, 60 and 90 min after tracer injection were collected, processed and analyzed for unmetabolized parent fraction with automatic column-switching HPLC system (2) equipped with a capture column (19 × 4.6 mm) packed with Phenomenex SPE C18 Strata-X sorbent (Torrance, CA, USA) and eluting with 1% acetonitrile in water at 2 mL/min. After 4 min the mobile phase was switched and activity trapped on the capture column was eluted onto a Phenomenex Gemini-NX column (250 × 4.6 mm, 5 μm) with 45% acetonitrile in 0.1M ammonium formate (pH 6.4) at a flow rate of 1.8 mL/min. The HPLC eluent was collected using an automated fraction collector (CF-1, Spectrum Chromatography). Activity in the blood, plasma, filtered plasma-urea mix, filters, and HPLC eluent fractions were counted with a gamma well-counter (Wizard 1480/ 2480, Perkin Elmer, Waltham, MA, USA). Typical HPLC profile for ¹¹C-LSN3172176 metabolite analysis is depicted in Supplemental Fig. 1. The unmetabolized parent fraction was determined as the ratio of the radioactivity corresponding to the parent (retention time of ~12 min) to the total amount of radioactivity collected, normalized to the recovery rate, which was determined by corresponding reference plasma samples and fitted with a bounded sum of exponential function. The final plasma input function was calculated as the product of the total plasma time activity curve (TAC) and the parent fraction curve.

An ultrafiltration-based method was used for measuring the unbound portion (free fraction, f_p) of ¹¹C-LSN3172176 in plasma in triplicate. About 100 μCi of ¹¹C-LSN3172176 in a volume no greater than 0.1 mL was added to 3.0 mL of arterial blood sample taken immediately before tracer injection. After ~5 min incubation at room temperature, the blood sample was centrifuged at 2,930 g for 5 min to separate the plasma. A 0.3 mL aliquot of plasma was loaded onto the Millipore Centrifree® micropartition device and centrifuged at 1,100 g for 20 min. The f_p was determined by calculating the ratio of the mean radioactivity concentration in the ultrafiltrate (unbound) to the mean total activity in plasma.

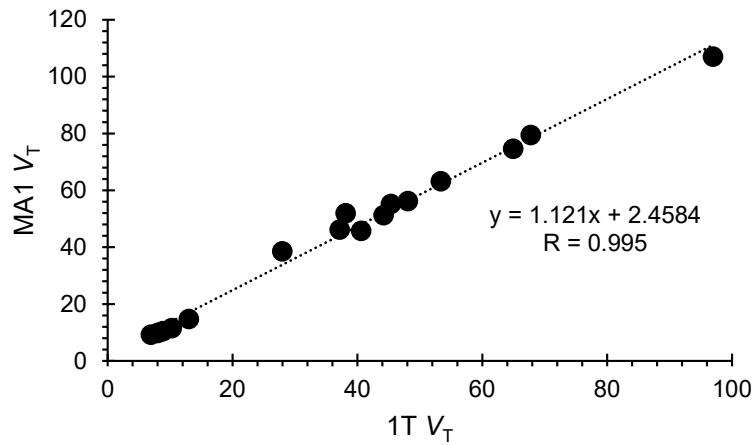
Supplemental Figure 1. Typical HPLC profile for ^{11}C -LSN3172176 metabolite analysis.

Log D was determined by the modified method from previously published procedures (3). ^{11}C -LSN3172176 (1 MBq) was added to a 2.0 mL microtube containing 0.8 mL 1-octanol and 0.8 mL 1X Dulbecco's phosphate buffered saline (PBS, pH=7.4). The mixture was vigorously vortexed for 20 s and centrifuged at 2,000 g for 2 min. A subsample of the octanol (0.2 mL) and PBS (0.7 mL) layers was counted in a gamma counter. The major portion of the octanol layer (0.5 mL) is diluted with 0.3 mL octanol and mixed with a fresh portion of 0.8 mL PBS. The distribution coefficient log D was determined by the ratio of activity in octanol and PBS. Value of log D was determined to be 2.96 ± 0.02 ($n=12$).

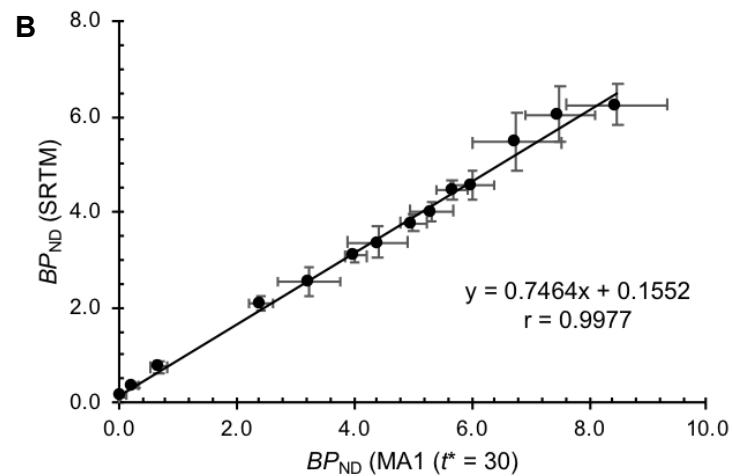
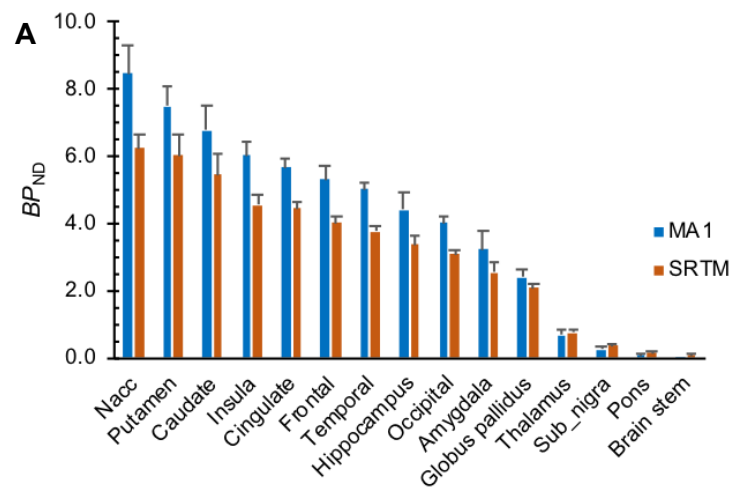
Kinetic Modeling

The 1T model was applied in conjunction with MA1 method (4) for comparison. The 1T model produced reliable V_T estimates with low standard errors (SE) and suitable fits. Supplemental Fig. 2 shows good correlation in regional V_T values between the two modeling methods.

Supplemental Figure 2. Comparison of V_T values from 1T and MA1 analyses.



Supplemental Figure 3. (A) Regional values of binding potential (BP_{ND}) for ^{11}C -LSN3172176 baseline scans ($n=4$) as estimated by MA1 and SRTM methods, using cerebellum as the reference region; (B) Correlation of MA1 and SRTM BP_{ND} values. Error bars are standard deviations



REFERENCES

1. Larsen P, Ulin J, Dahlstrøm K, Jensen M. Synthesis of ^{11}C -iodomethane by iodination of ^{11}C -methane. *Appl Radiat Isot.* 1997;48:153-157.
2. Hilton J, Yokoi F, Dannals RF, Ravert HT, Szabo Z, Wong DF. Column-switching HPLC for the analysis of plasma in PET imaging studies. *Nucl Med Biol.* 2000;27:627-630.
3. Wilson AA, Jin L, Garcia A, DaSilva JN, Houle S. An admonition when measuring the lipophilicity of radiotracers using counting techniques. *Appl Radiat Isot.* 2001;54:203-208.
4. Ichise M, Toyama H, Innis RB, Carson RE. Strategies to improve neuroreceptor parameter estimation by linear regression analysis. *J Cereb Blood Flow Metab.* 2002;22:1271-1281.